NAVAL POSTGRADUATE SCHOOL
Monterey, California

THESIS

STIMULATED CERENKOV RADIATION BEAM MONITOR

by

Kenneth Scott Pugh

June 1983

Thesis Advisor: F.R. Buskirk

Approved for public release; distribution unlimited

SECURITY CLASSIFICATION OF THIS PAGE *(When Data Entered)*

REPORT DOCUMENTATION PAGE

READ INSTRUCTIONS BEFORE COMPLETING FORM

1. REPORT NUMBER	2. GOVT ACCESSION NO. / 3. RECIPIENT'S CATALOG NUMBER
4. TITLE *(and Subtitle)*: STIMULATED CERENKOV RADIATION BEAM MONITOR	5. TYPE OF REPORT & PERIOD COVERED: Master's Thesis; June 1983
	6. PERFORMING ORG. REPORT NUMBER
7. AUTHOR(s): Kenneth Scott Pugh	8. CONTRACT OR GRANT NUMBER(s)
9. PERFORMING ORGANIZATION NAME AND ADDRESS: Naval Postgraduate School, Monterey, California 93940	10. PROGRAM ELEMENT, PROJECT, TASK AREA & WORK UNIT NUMBERS
11. CONTROLLING OFFICE NAME AND ADDRESS: Naval Postgraduate School, Monterey, California 93940	12. REPORT DATE: June 1983
	13. NUMBER OF PAGES: 66 pages
14. MONITORING AGENCY NAME & ADDRESS *(if different from Controlling Office)*	15. SECURITY CLASS. *(of this report)*: Unclassified
	15a. DECLASSIFICATION/ DOWNGRADING SCHEDULE

16. DISTRIBUTION STATEMENT *(of this Report)*

Approved for public release; distribution unlimited

17. DISTRIBUTION STATEMENT *(of the abstract entered in Block 20, if different from Report)*

18. SUPPLEMENTARY NOTES

19. KEY WORDS *(Continue on reverse side if necessary and identify by block number)*

Stimulated Cerenkov Radiation
Beam Monitor

20. ABSTRACT *(Continue on reverse side if necessary and identify by block number)*

It has been suggested that many important characteristics of a bunched relativistic electron beam might be determined by monitoring the Cerenkov radiation produced as the beam passes through or very close to a dielectric medium. This report describes an effort to produce stimulated Cerenkov radiation (SCR) in a dielectric slab using a bunched beam of 100 MEV electrons from a linear accelerator. Although the method used displayed only limited success, the results were consistent with previous work

DD FORM 1 JAN 73 1473 EDITION OF 1 NOV 65 IS OBSOLETE

S/N 0102-LF-014-6601

SECURITY CLASSIFICATION OF THIS PAGE *(When Data Entered)*

20. (Continued)

and further confirmed the basic ideas regarding SCR production.

In conjunction with the experimental work performed, an analysis was conducted concerning the manner in which various electron charge distributions which might be used to describe how the electron bunches affect the Cerenkov radiation emitted by the beam. In principle, the results imply that proper monitoring of the Cerenkov radiation from a beam should allow one to deduce the total bunch charge and charge distribution.

Approved for public release; distribution unlimited

Stimulated Cerenkov Radiation Beam Monitor

by

Kenneth Scott Pugh
Lieutenant, United States Navy
B.S., U.S. Naval Academy, 1976

Submitted in partial fulfillment of the
requirements for the degree of

MASTER OF SCIENCE IN PHYSICS

from the

NAVAL POSTGRADUATE SCHOOL
June 1983

ABSTRACT

It has been suggested that many important characteristics of a bunched relativistic electron beam might be determined by monitoring the Cerenkov radiation produced as the beam passes through or very close to a dielectric medium. This report describes an effort to produce stimulated Cerenkov radiation (SCR) in a dielectric slab using a bunched beam of 100 MEV electrons from a linear accelerator. Although the method used displayed only limited success, the results were consistent with previous work and further confirmed the basic ideas regarding SCR production.

In conjunction with the experimental work performed, an analysis was conducted concerning the manner in which various electron charge distributions which might be used to describe how the electron bunches affect the Cerenkov radiation emitted by the beam. In principle, the results imply that proper monitoring of the Cerenkov radiation from a beam should allow one to deduce the total bunch charge and charge distribution.

TABLE OF CONTENTS

ACKNOWLEDGEMENT

The author wishes to express his gratitude to his advisors, Professors Fred R. Buskirk and John R. Neighbours for the guidance and direction they provided. The assistance given by Mr. Don Snyder, who operated the linear accelerator and did much of the work required to set up the apparatus, is also greatly appreciated.

I. INTRODUCTION

A charged particle which passes through or sufficiently close to a medium at a speed greater than that of light in the material will act together with the particles in the medium to produce a continuous spectrum of electromagnetic radiation. Although this effect was observed earlier by others, P. A. Cerenkov is recognized for his work in 1934 as having discovered and in 1937, together with I. M. Frank and I. E. Tamm, being first to correctly describe the process producing what is now referred to as Cerenkov radiation. Until as recently as the late 1970's this form of radiation has received comparatively little study, with the emphasis during the intervening years being placed upon the exigent development of radiation sources and uses in the radio, radar and most recently, microwave regions of the spectrum. It now appears that technologies developed during these years have been advanced to their useful limits in the effort to produce radiation sources in the millimeter wavelength (and shorter) regions of the spectrum. Sources, especially tuneable ones, in this region would allow the progress of major developments in communications, plasma and fusion physics, medicine and other fields. It is this need for millimeter wavelength sources which has renewed interest

in the study of Cerenkov radiation. Recent results of J. E. Walsh and others working at Dartmouth have shown that it is possible to produce millimeter radiation at high power levels using an intense relativistic electron beam and a dielectric resonator in a cylindrical waveguide [Ref. 1]. In this method, the beam interacts with the dielectric to produce Cerenkov radiation and in turn is effectively coupled to the waveguide modes occupied by the Cerenkov radiation as it propogates within the waveguide. The coupling allows some beam energy to be transferred to the waveguide modes which are thus amplified. Although the Cerenkov spectrum in continuous (it does not however include the x-ray and gamma ray or shorter regions of the spectrum) [Ref. 2: p. 6] and its energy will reside in many waveguide modes at differing frequencies, it is peaked in a particular mode. This was shown theoretically by Abele in 1952 [Ref. 3: p. 63]. Abele also showed that for the case being considered,

$$W_n \propto Z^2 \tag{1}$$

where W_n is the power in the peak power mode and Z is the interaction distance. This means that longer interaction distances have the effect of shifting the power from many waveguide modes into the peak power mode. Consistent with Abele's findings, Walsh also showed that the frequency

favored by the resonator depends only on its geometry and material properties, suggesting that a proper choice of these parameters would allow generation of radiation at any practical wavelength within the Cerenkov spectrum. One experiment conducted by Walsh's group obtained 1MW peaked at 60GHZ (5mm) [Ref. 4].

A separate effort to develop a tuneable source of short wavelength radiation which has been studied and tested with some success involves the free electron laser (FEL). For the reader unaquainted with the FEL, its theory of operation is available in many references. For this purpose, it is adequate to say that such a device uses a magnetic field which varies spatially, temporally, or in both ways, to perturb or wiggle the trajectories of electrons in a highly relativistic beam in such a way as to produce coherent radiation. The beam used in the FEL and in the Cerenkov resonator must be bunched in order to produce net radiation. In practice, the correct bunching of the beam may be critical to successful FEL operation.

This state of affairs prompted the suggestion by F. R. Buskirk that it should be feasible to utilize the beam-to-dielectric coupling scheme demonstrated at Dartmouth in a beam monitor application with the purpose of obtaining diagnostic information about the beam relevant to its use in an FEL. Initial testing of a prototype resonator was

performed by L. J. Brown and D. E. McLaughlin [Ref. 5,6]. In the present experiment, different materials and resonator geometries were tested to learn more about the methods to produce stimulated Cerenkov radiation (SCR) to monitor a bunched electron beam from a linear accelerator.

In a recently published report, F. R. Buskirk and J. R. Neighbours [Ref. 7] analyzed the production of Cerenkov radiation by a bunched beam in air rather than in a waveguide. Their work was concerned with the effects of finite interaction regions and bunch characteristics on such parameters as radiated power, Cerenkov angle spreading and behavior at high frequencies. Also addressed was an approach to determine the effects of bunch charge distribution on the radiated power spectrum. Preliminary corroborating results were obtained by A. Saglam [Ref. 8]. In this paper the methods developed by Buskirk and Neighbours are used to determine the expected effects on the Cerenkov radiation emitted by a bunched beam by a number of specific possible bunch charge distributions.

II. THEORY

A. SCR WAVEGUIDE MODES

McLaughlin solved the boundary value problem which gives the frequencies to be expected from a hypothetical infinite slab resonator coupled to a relativistic beam. The physics of this boundary value problem are fundamental to the understanding of the resonator, therefore it is summarized below. The complete derivation can be found in McLaughlin's thesis. [Ref. 5: p. 11-24]

Figure 1 shows the dielectric slab used in the experiment. For the purpose of the theory, the slab is considered to be finite in thickness while extending to infinity in its other two dimensions. One side of the slab is in contact with a perfect conductor and the space surrounding the slab is a perfect vacuum. An infinitely long bunched electron beam propagates parallel to the plane of the slab just slightly above the side opposite the perfect conductor. Now suppose an electromagnetic wave propagates through the slab without attenuation and parallel to the direction of the electron beam. The origin of this wave will be considered later. Although the wave disturbance exists within the dielectric slab, Maxwell's equations require the presence of an evanescent wave which extends beyond the surface of the

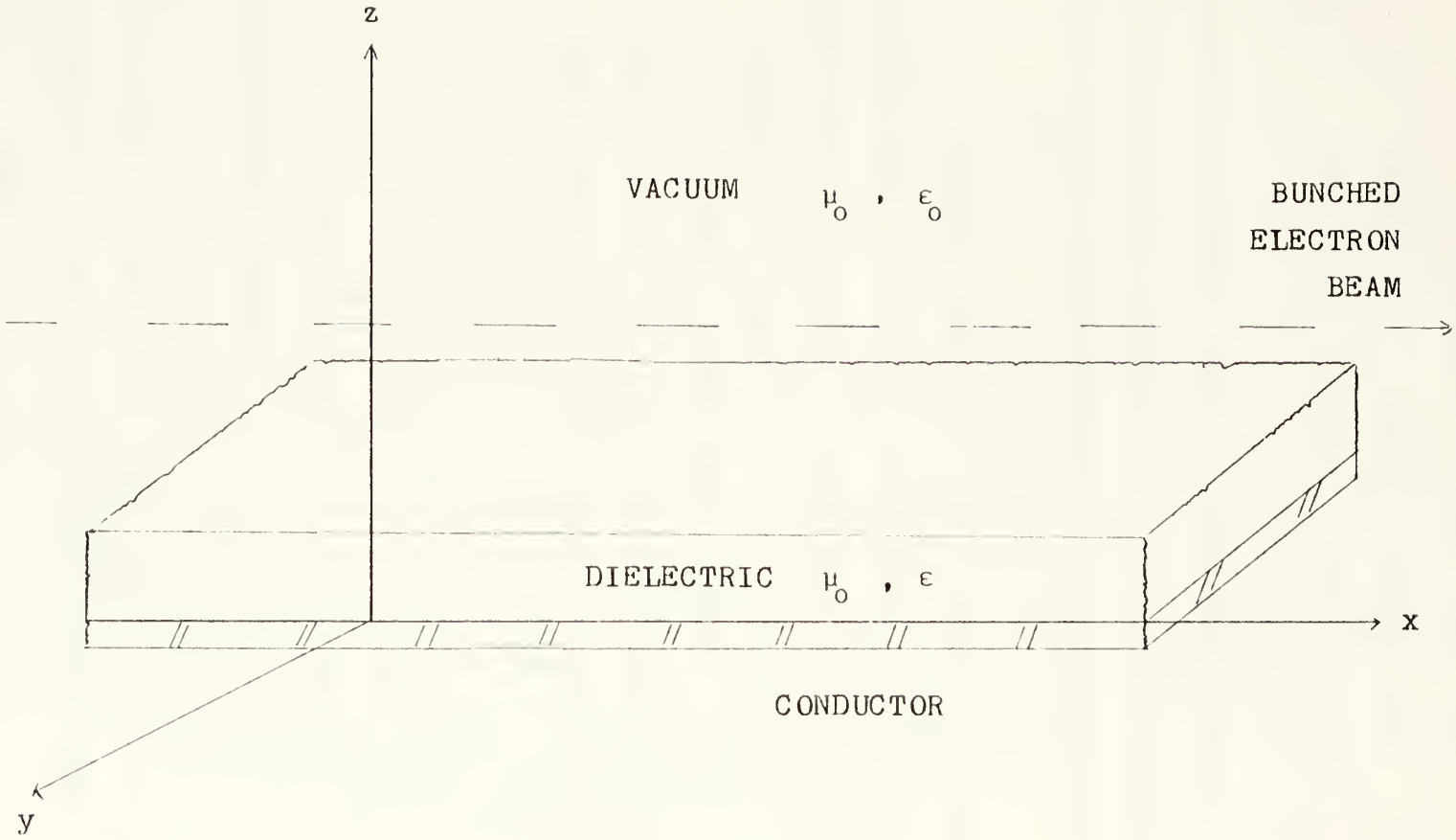

INFINITE DIELECTRIC SLAB

FIGURE 1

slab [Ref. 9: p. 48-49]. The phase velocity of the wave will depend on the slab refractive index, the wave frequency, the slab thickness and the particular mode. In a manner similar to that which occurs in a hollow metal waveguide, the wave may exist in any combination of the allowed transverse magnetic (TM) or transverse electric (TE) modes for the particular frequency and geometry. Since the beam and wave have the same direction, if a TM mode is present, as it should be, then this mode will have a component of its electric field in the direction of the beam. This means that electrons in the beam will be able to exchange energy with the wave in a way analogous to the beam-wave exchange in the familiar klystron tube, traveling wave tube or in the linear accelerator (LINAC) itself where a reverse process allows the waves to give energy to the electrons. Under these conditions then, if the dielectric thickness is such as to produce a TM mode having a phase velocity matching that of the beam electrons, the energy in this mode will grow if proper phasing is provided between the wave and the bunches of electrons. Note that the beam must be bunched since electrons in a continuous beam would contribute energy to certain parts of the wave while subtracting an equal amount from other parts on the average. McLaughlin showed that the frequency which experiences the exchange with the beam is

$$f = \frac{1}{2\pi l\left(\mu_o\epsilon - \frac{1}{\beta^2c^2}\right)^{1/2}}\left\{m\pi + \tan^{-1}\left[n^2\left(\frac{\frac{1}{\beta^2c^2} - \mu_o\epsilon_o}{\mu_o\epsilon - \frac{1}{\beta^2c^2}}\right)^{1/2}\right]\right\} \quad (2)$$

where m (=0,1,2,3....) is the waveguide mode, l is the slab thickness, n is the index of refraction, $\beta = \frac{v}{c}$ (where v is the velocity of electrons in the beam and c is the speed of light in vacuum), and ϵ is the dielectric constant of the slab material. Using

$$n = \sqrt{\frac{\epsilon}{\epsilon_o}} \quad , \quad \mu_o\epsilon = \left(\frac{n}{c}\right)^2 \quad , \quad \mu_o\epsilon_o = \left(\frac{1}{c}\right)^2$$

equation (2) can be expressed as

$$f = \frac{c}{2\pi l\left(n^2 - \frac{1}{\beta^2}\right)^{1/2}}\left\{m\pi + \tan^{-1}\left[n^2\left(\frac{\frac{1}{\beta^2} - 1}{n^2 - \frac{1}{\beta^2}}\right)^{1/2}\right]\right\} \quad (3)$$

where n and l are the slab properties defined earlier and β is a beam property.

The electron velocities from the LINAC are most closely matched to the m=1 mode phase velocity. McLaughlin's attempt to demonstrate such a one-to-one correspondence between electron energy and slab frequency was not successful. This was probably due to the disparity between the assumptions made regarding the infinite slab and the

actual slab, in addition to other problems discussed later. The 20cm long slab used by McLaughlin is roughly twice the separation between electron bunches in the beam. The beam is described in greater detail in Appendix A.

In a paper written subsequent to McLaughlin's, L. J. Brown addressed the problems posed in applying the infinite slab theory to the finite slab [Ref. 6: p. 12-14]. Brown makes the case that although a finite interaction distance is used, energy exchange is still expected for that frequency having a phase velocity equal to that of the electrons. This would also be true for other frequencies close to this "tuned frequency". At the "tuned frequency", the wave stays exactly in phase with the electron, assuring that energy is given to the mode, assuming the correct initial phase, so that gain occurs. Now consider an electron interacting with a mode near the tuned frequency. If the phase is initially correct for gain, as the electron and mode move, the phase will not remain correct for gain. However, for a finite length of resonator, the phase change downstream may be small, so that the gain is still close to maximum. Of course, if a relative shift of one or any integer number of complete cycles were to occur, net energy transfer would be forbidden. Brown's argument leads us to expect the finite slab to produce SCR but does not account for the difficulties encountered by McLaughlin in detecting the tuned frequency. We shall return to this matter later.

In order to consider the wave-beam interaction, the presence of a wave was assumed. Its existence must be real in order for the experiments of Walsh to have been successful. Turning our attention to the origin of this wave, Walsh's associate, K. L. Felch [Ref. 3: p. 71] offered the following explanation. Although his remarks were intended to apply to a cylindrical resonator, they can be extended to apply to a slab which can be thought of as a strip of a thin-walled cylinder. As the electrons pass near the dielectric, a small amount of ordinary Cerenkov radiation is produced. This radiation is reflected back and forth inside the dielectric corresponding to the modes dictated by the system geometry and material properties. These fields then interact with the electrons so as to speed up some while slowing others down. If more electrons are slowed than sped up, the fields gain energy.

B. AIR CERENKOV

In their treatment of the subject Cerenkov radiation from a bunched relativistic electron beam in air (the results apply for any nondispersive dielectric), F. R. Buskirk and J. R. Neighbours consider the type of emission to be expected when a finite interaction distance exists as opposed to the well know results of Jelly and others [Ref. 3: p. 3-7] which were for the case of a single charged particle moving at constant speed in an infinite medium

which produces the familiar cone of Cerenkov radiation. Buskirk and Neighbours showed that [Ref. 7: p. 13] the radiated power for this situation is given by

$$P_\omega = \frac{\mu}{4\pi} \omega v^2 \sin^2 \theta_c \left| \tilde{\rho}_o (\vec{k}) \right|^2 4\pi \frac{Z'}{Z^2} \qquad (4)$$

where

ω = a harmonic of the bunch angular frequency ω_o

v = electron velocity

θ_o = usual Cerenkov angle $\cos^{-1} \left(\frac{1}{\beta n} \right)$

Z' = 1/2 the pulse length or interaction distance

Z = spacing between electron bunches

$\tilde{\rho}_o(\vec{k})$ = three dimensional fourier transform of the single bunch charge density.

Now we recognize that the ratio of interaction distance to bunch spacing $2Z'/Z = N$, the number of bunches present in the interaction length. Also, the bunch spacing can be expressed as $Z = v2\pi/\omega_o$ where ω_o is the bunch repetition frequency. Making these substitutions, (4) becomes

$$P_\omega = \frac{\mu}{4\pi} \omega \omega_o v \sin^2 \theta_c \left| \tilde{\rho}_o(\vec{k}) \right|^2 N \qquad (5)$$

To compare with usual formulations, (5) is divided by the quantity Nv to obtain energy loss per unit length per bunch. This gives

$$\frac{dE}{dx} = \frac{\mu}{4\pi} \omega\omega_o \sin^2 \theta_c \left| \underset{\sim}{\rho}_o(\vec{k}) \right|^2 \qquad (6)$$

The effects of bunch charge and charge distribution (size and shape) on P_ω are felt through $\underset{\sim}{\rho}_o(\vec{k})$. To examine this effect, we define the charge form factor $F(\vec{k})$ in the following manner:

$$\underset{\sim}{\rho}_o(\vec{k}) = q\, F(\vec{k}) \qquad (7)$$

where q is the total charge in an individual bunch. Thus

$$F(\vec{k}) = \frac{1}{q} \iiint d^3r\ \rho(\vec{r})\ e^{i[\vec{k} \cdot \vec{r}]} \qquad (8)$$

For the case when $|\vec{k}| = \frac{\omega}{c} = 0$ we find

$$F(\vec{k}=0) = \frac{1}{q} \iiint d^3r\ \rho(r) = 1 \quad \text{identically.} \qquad (9)$$

For the example of a point charge $F(\vec{k}) = 1$ for all values of $\vec{k}$. Using (7) we rewrite (5) as follows to include q and $F(\vec{k})$ explicitly:

$$P = \frac{\mu}{4\pi} \omega\omega_o v \sin^2 \theta_c\, q^2\, F^2(\vec{k})\, N \qquad (10)$$

Since the actual bunches produced by a LINAC are not point charges but have some distribution in space, let us consider the next simplest imaginable case, that of

spherical bunches having uniform charge density ρ_o and radius r_o.

Let $\vec{k} \cdot \vec{r} = kru$, where u is the cosine of the angle between $\vec{k}$ and $\vec{r}$. In spherical coordinates,

$$d^3r = r^2 \sin\theta dr d\theta d\phi = r^2 dr du d\phi$$

Thus,

$$F(k) = \frac{\iiint e^{ik\cdot r}\, \rho(\vec{r})\, d^3r}{\iiint \rho(\vec{r})\, d^3r} = \frac{2\pi \iint e^{ikru}\, \rho_o\, r^2 du dr}{q} \qquad (11)$$

$$= \frac{2\pi}{q} \rho_o \int_0^{r_o} r^2 \left[\left(\frac{1}{ikr}\right) e^{ikr} - e^{-ikr}\right] dr$$

$$= \frac{4\pi}{q} \rho_o \int_0^{r_o} r^2 \left[\frac{\sin kr}{kr}\right] dr$$

$$= \frac{4\pi}{qk} \rho_o \int_0^{r_o} r \sin kr\, dr \qquad (12)$$

If we require $|\vec{k}|$ small (low frequency) then,

$$F(k) = \frac{4\pi}{qk} \rho_o \int_0^{r_o} r \left(kr - \frac{k^3 r^3}{3!} + \ldots\right) dr$$

$$F(k) = \frac{4\pi\rho_o}{q}\left[\frac{r^3}{3} - \frac{k^2}{6}\int_0^{r_o} r^2 r^2 dr\right]$$

$$= 1 - \frac{k^2}{6}\langle r^2\rangle$$

where $\langle r^2\rangle$ is the mean square radius of the bunch. On the other hand, if we impose no restrictions on k then (12) is evaluated differently as follows:

$$F(k) = \frac{4\pi\rho_o}{k\frac{4}{3}\pi r_o^3\rho_o}\int_0^{r_o} r \sin kr\, dr$$

$$= \frac{3}{(kr_o)^3}\left[\frac{1}{k^2}\sin kr - \frac{r}{k}\cos kr\right]_{r=0}^{r=r_o}$$

$$= \frac{3}{(kr_o)^3}\left[\sin kr_o - kr_o \cos kr_o\right] \qquad (13)$$

It is easily shown that $\lim_{\vec{k}\to 0} F(\vec{k}) = 1$ as required. A plot of this function is shown in Figure 2. If we return to (10) and use $|\vec{k}| = \frac{\omega}{v}$ we can express the power radiated by the spherical bunches of uniform charge density as

$$P_\omega = \frac{\mu}{4\pi}\omega_o v \sin^2\theta_c\, q^2\, N\omega \left\{3\left(\frac{v}{\omega r_o}\right)^3\left[\sin\frac{\omega r_o}{v} - \frac{\omega r_o}{v}\cos\frac{\omega r_o}{v}\right]\right\}^2 \qquad (14)$$

Figure 3 is a plot of this function.

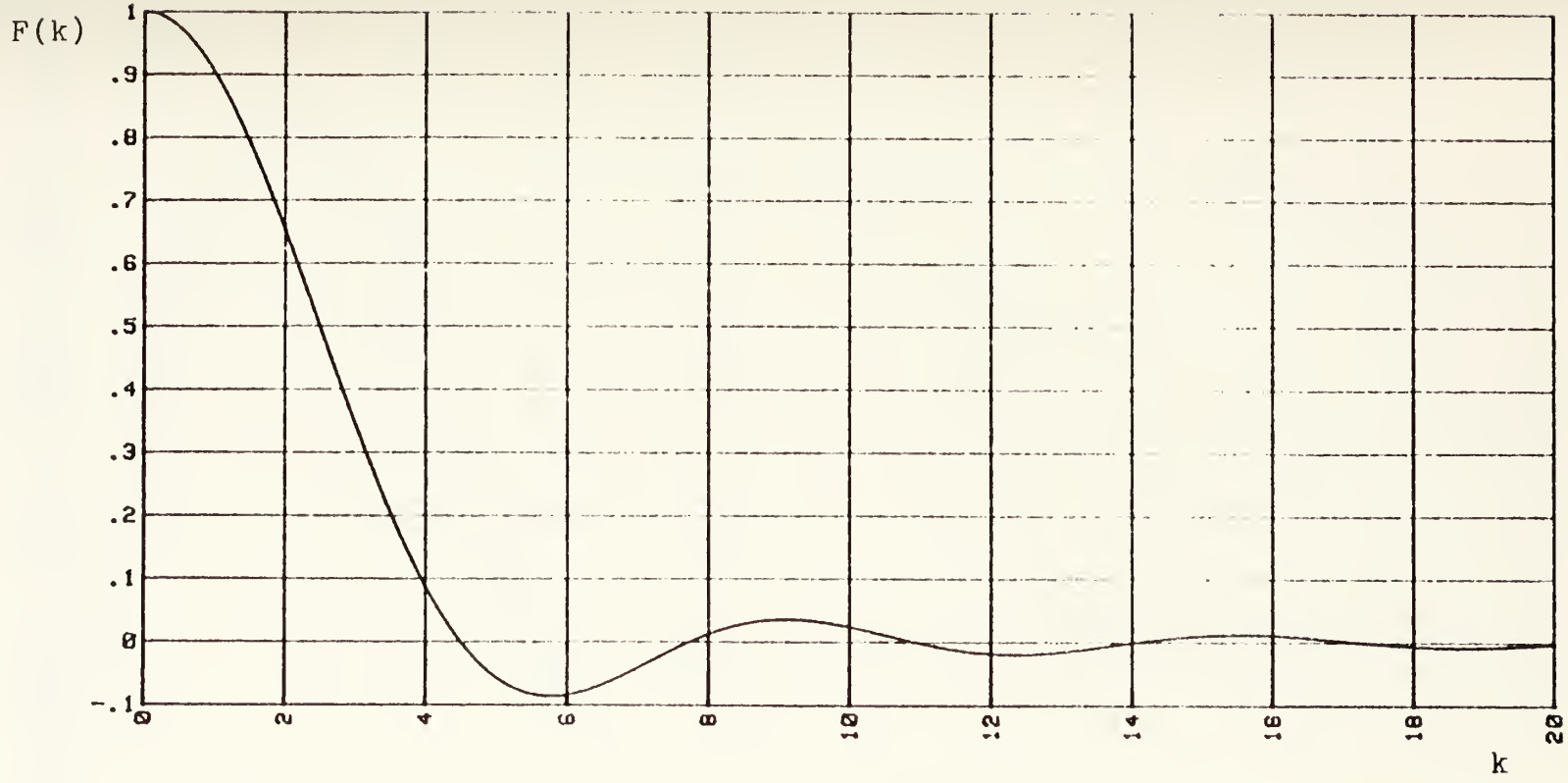

UNIFORM SPHERICAL BUNCH FORM FACTOR

FIGURE 2

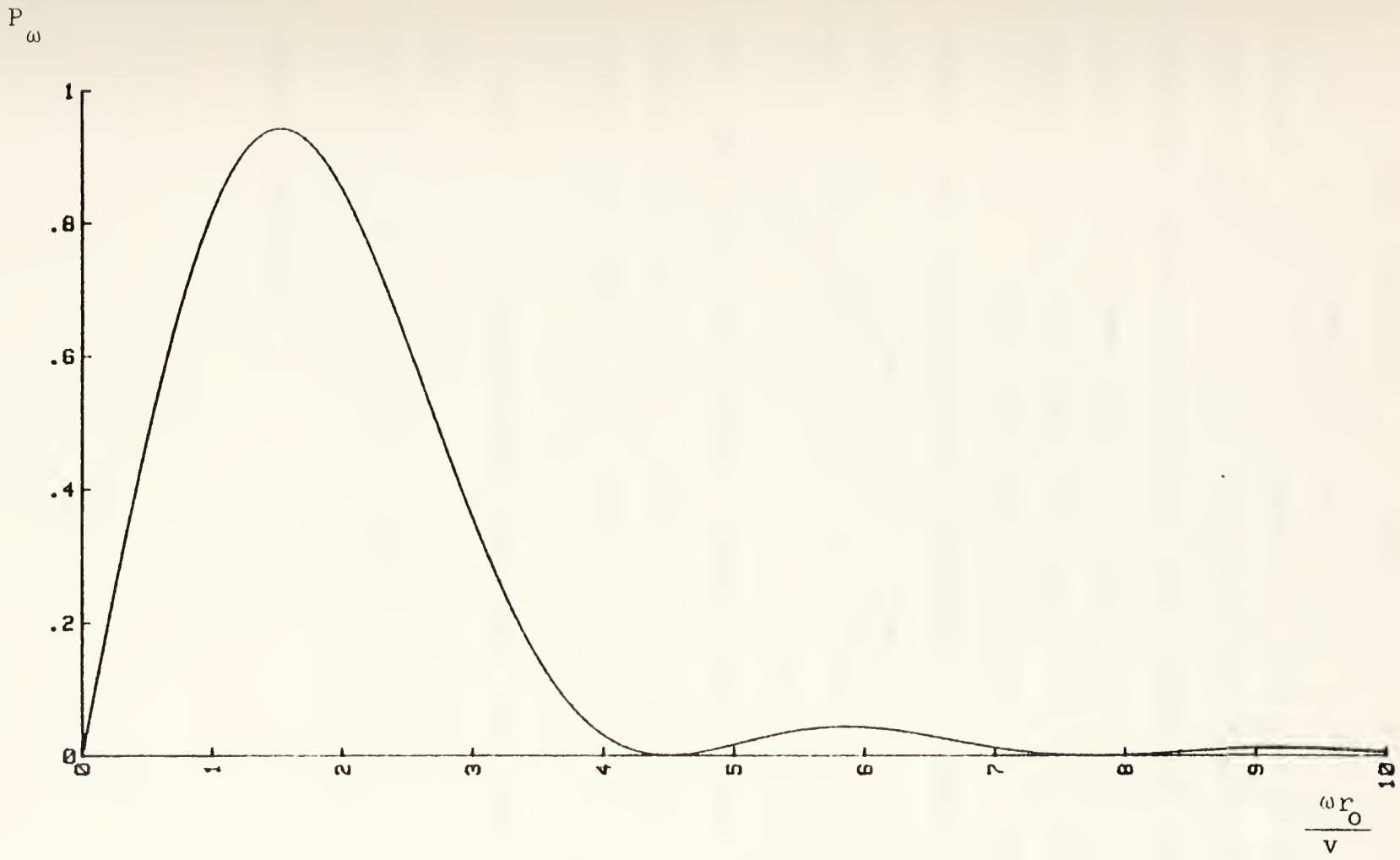

UNIFORM BUNCH RADIATED POWER

FIGURE 3

We can investigate the effect of bunch charge distribution on emitted power further if we consider other examples. We choose as reasonable illustrative examples bunches which have radial charge distributions described by Gaussian, cosine and spherical shell functions but all of which have the same spherical shape. We then proceed as before to find the respective form factors and power expressions. Since the method is identical to that used above, the calculations are included in Appendix B to avoid repetition. In order to allow a meaningful comparison of the results for the various distributions, the calculations were performed so that in spite of their different charge distributions, the Gaussian, cosine and spherical shell bunches each enclosed the same total charge and have the same actual size as the uniform bunch described earlier. This effectively normalizes the calculation results with respect to the uniform bunch and means that the quantity $\frac{\mu}{4\pi}\,\omega_o\, v \sin^2\theta_c\, q^2 N$ in (10) is the same in all cases. Figures 4 through 6 may be compared to Figure 3 to assess the effect of varying the charge distribution for the bunch types considered.

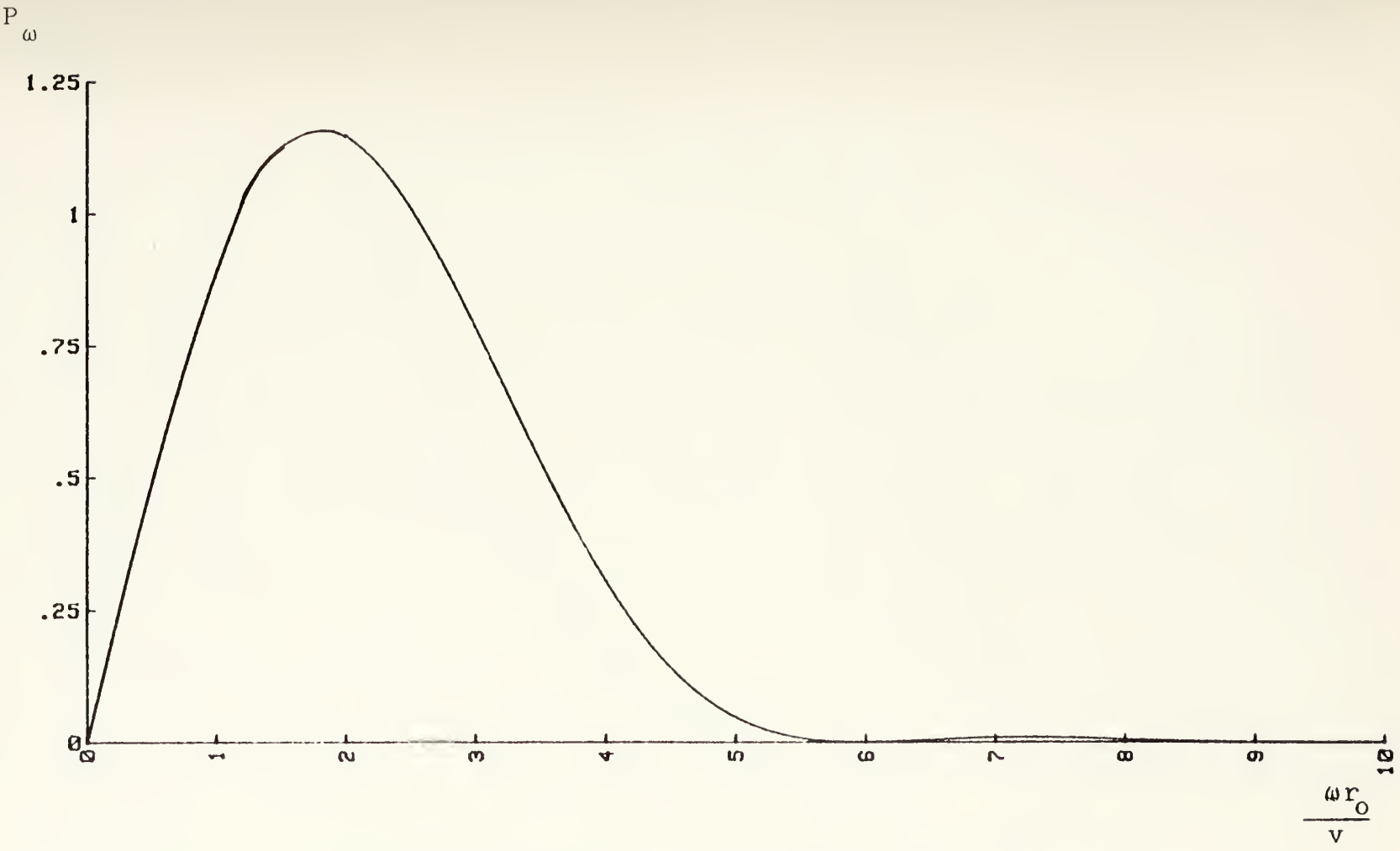

COSINE BUNCH RADIATED POWER

FIGURE 4

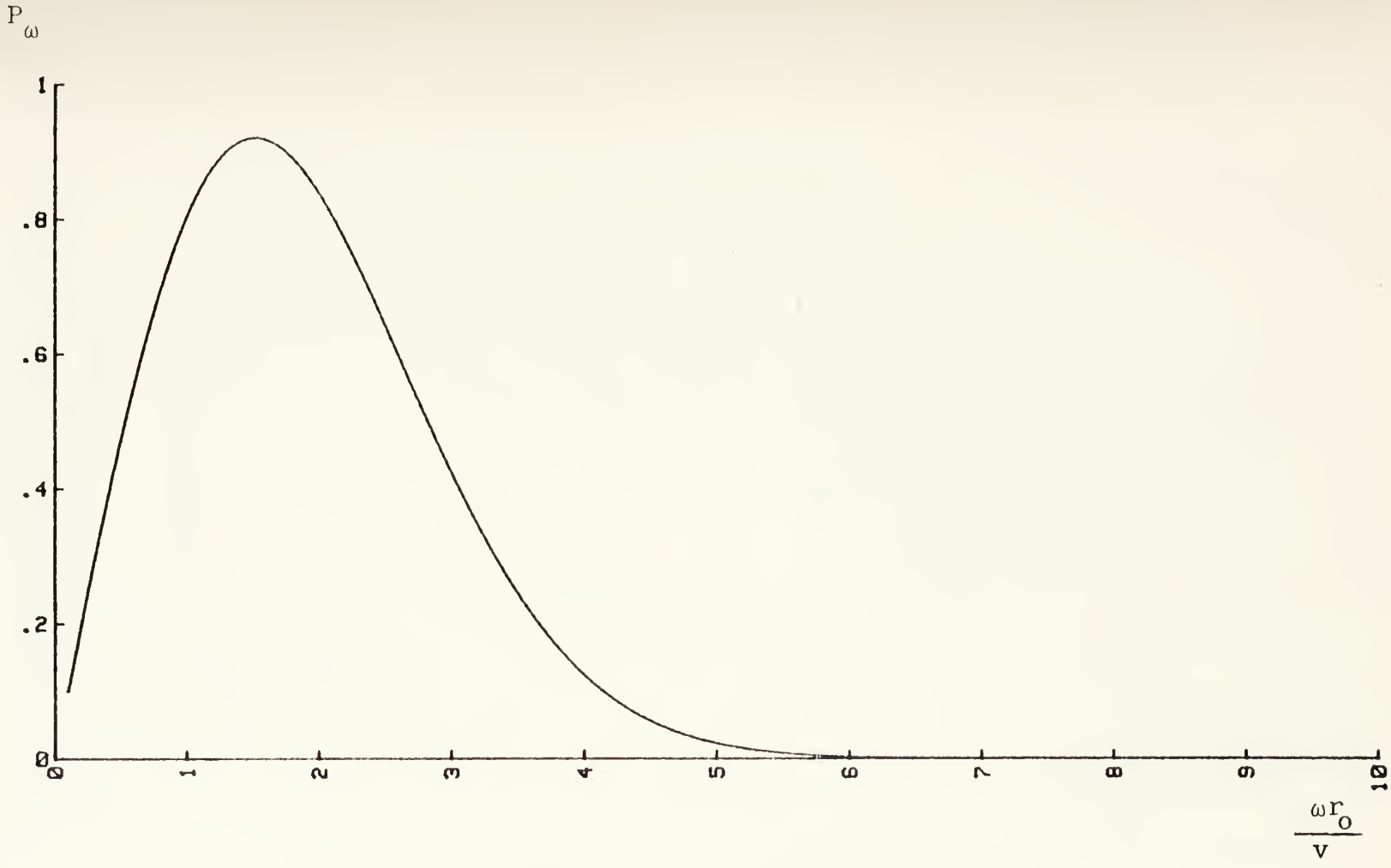

GAUSSIAN BUNCH RADIATED POWER

FIGURE 5

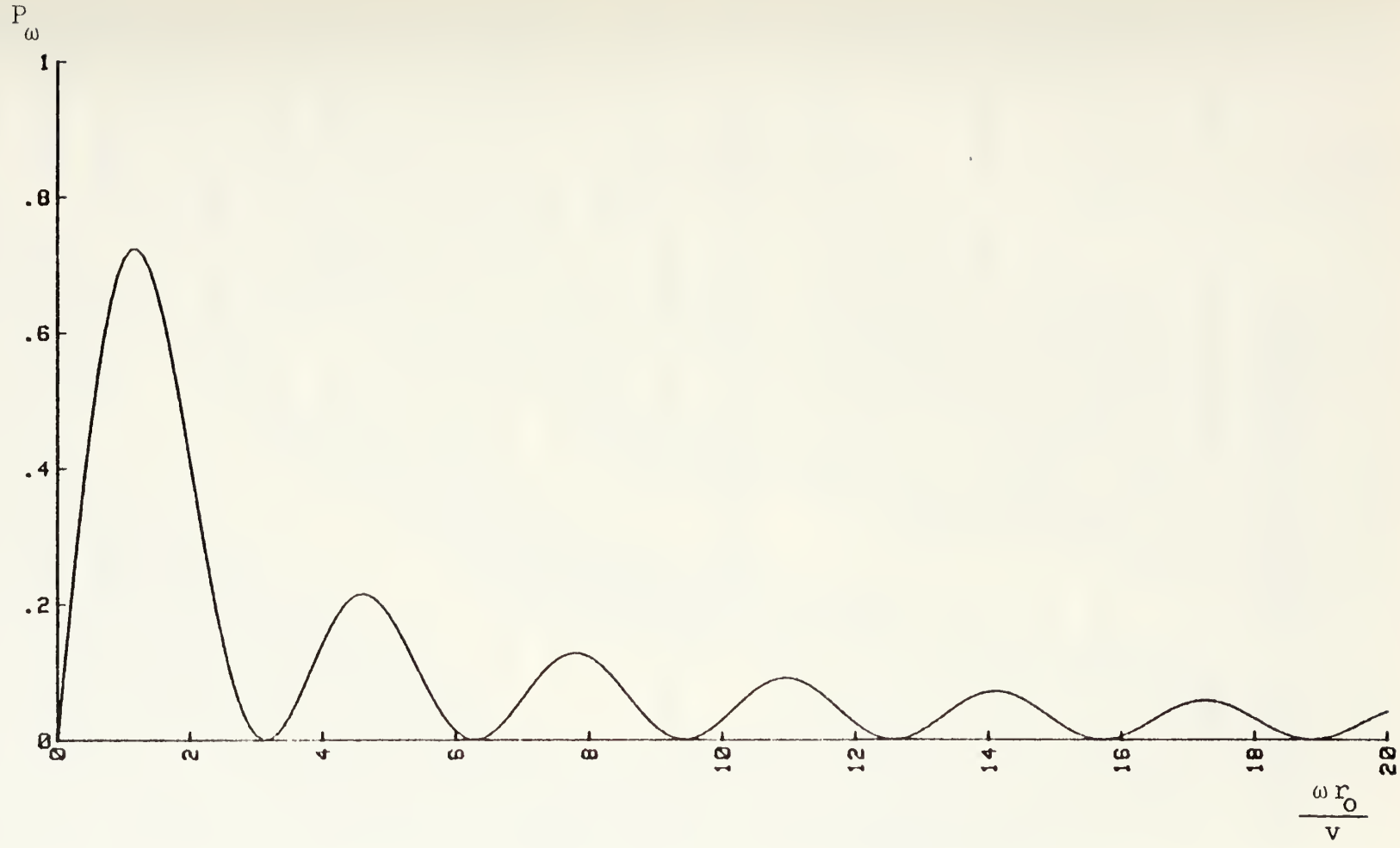

SPHERICAL SHELL BUNCH RADIATED POWER

FIGURE 6

III. EXPERIMENTAL PROCEDURE AND RESULTS

The initial experimental setup is shown in Figure 7. The dielectric resonator slab was 1/2 inch thick, 20cm long and 5cm wide. The material used, STYCAST 0005, is a commerically available dielectric used in microwave engineering applications and has a relative dielectric constant of 2.54 and low attenuation in the frequency range of interest. As can be seen in Figure 7 the slab design incorporated a 20 degree bend.

A. REVIEW OF PREVIOUS EXPERIMENTS

In the original experiments of McLaughlin a straight slab was used. To analyze the signal from the slab, a Tektronix Type 491 Spectrum Analyzer (S/A) was used. Due to radiation level in the LINAC target area, the S/A had to be located in the control room to allow personnel access. For this reason approximately 75 feet of X-band waveguide were required to connect the slab to the S/A. The waveguide introduced far less attenuation at the frequencies used than coaxial cable, however it did have a cutoff frequency of 6.56 GHZ. The end of the 5cm wide slab was tapered in width and thickness to fit into the open end of the X-band waveguide. This was to facilitate the transmission of microwave radiation from the slab into the waveguide.

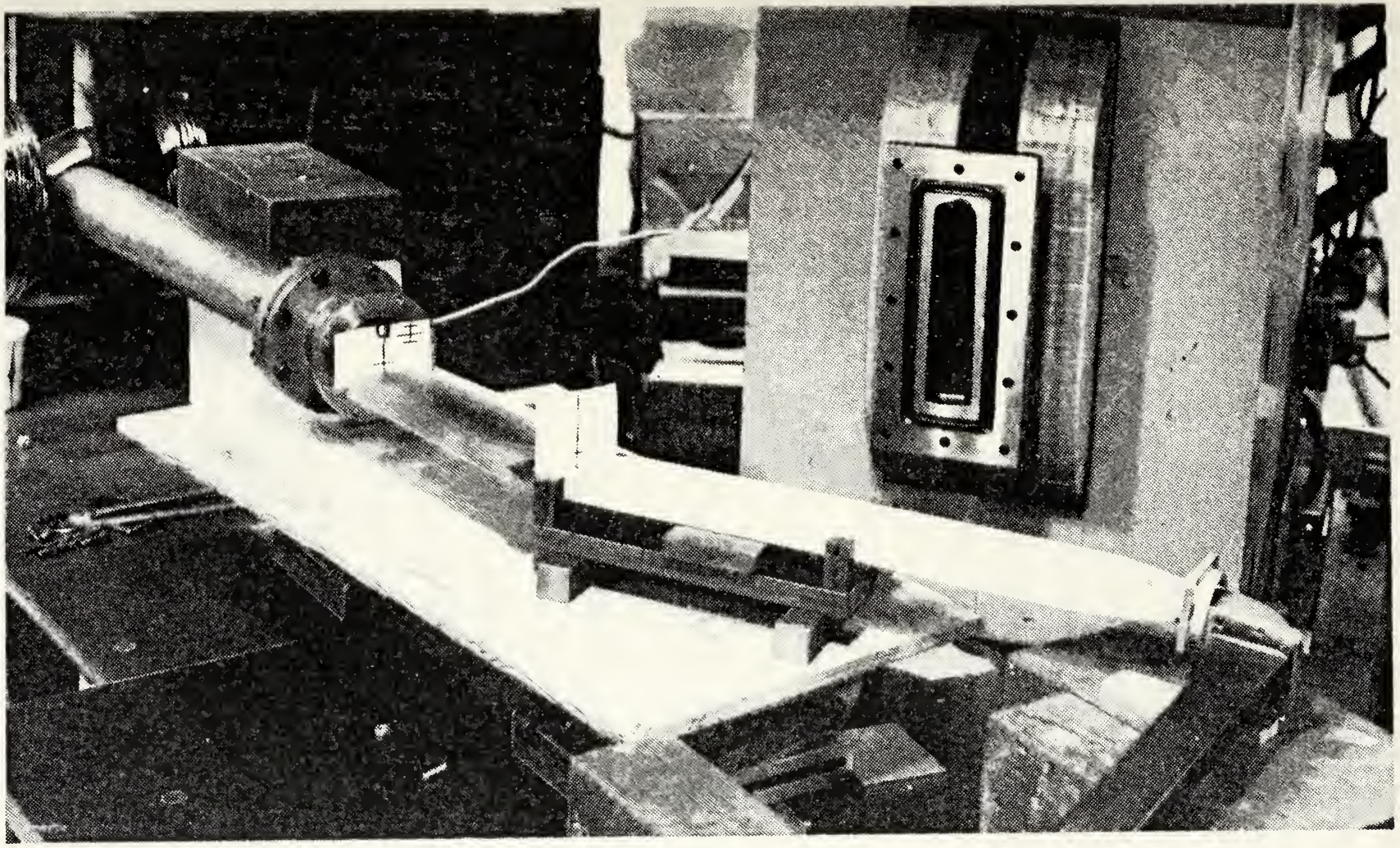

EXPERIMENTAL SETUP

FIGURE 7

McLaughlin found that with the beam on, he obtained a weak signal at the S/A regardless of whether the slab was in place. He reasoned that the signal being detected was not exclusively SCR from the slab but must be air Cerenkov from the beam which entered the waveguide opening. It is relevant to note that since a similar signal was detected with the slab in place, the air Cerenkov easily propagated through the STYCAST slab. At standard conditions air has a refractive index of 1.0003 meaning that the Cerenkov threshold obtained from

$$1 = \frac{1}{\beta n}$$

corresponds to $\beta = .9997$ or approximately 21 Mev for an electron.

To test his idea, McLaughlin enclosed the slab in a box which could be evacuated to eliminate the air. Again a weak signal was observed which did not change when the slab was removed from the vacuum box. In this case it was concluded that the aluminum box was resonating since it had transverse dimensions on the order of a few wavelengths at the expected frequency.

Brown suggested that it was probable that the open end of the waveguide would respond as an antenna to the bunched electron beam passing near it. This was the reason for the

first use of the 20 degree bend since it would allow the takeoff end of the waveguide to be removed from the path of the beam by several wavelengths. The vacuum box would have required a difficult modification to accommodate the bend and it was decided to eliminate it altogether to avoid the unwanted cavity modes produced by the metallic box. The first tests of the 20 degree bend slab yielded several detectable signals which did not persist when the slab was removed. It is known that the discontinuity between a material of high dielectric constant (e.g., the dielectric slab) and another of lower dielectric constant makes it possible to confine an electromagnetic wave within the material of higher constant [Ref. 9: p. 225]. It seemed possible therefore that the observed signal might be SCR from the slab, air Cerenkov which entered the slab and was ducted into the waveguide in the fashion described above, or any combination of these possibilities. To resolve this point, Brown enclosed the entire apparatus in a large plastic bag which was kept purged with helium and vented at its lowest point. This step eliminated the air without introducing the problems posed by a vacuum box. At 1.000033 the refractive index of helium gives a Cerenkov threshold of 63 Mev. With the LINAC operating at 30 Mev (see Appendix A for an explanation of LINAC capabilities) Brown obtained a slightly stronger signal when the helium was used than when

the identical experiment was performed in air although both signals were weak relative to the minimum sensitivity of the S/A. The result supported the conclusion that the detected signal was indeed SCR and not air Cerenkov although the effects of reduced beam spreading in helium were not thoroughly investigated nor was it possible to confirm the purity of the helium used.

B. PROCEDURE

The difficulties encountered by McLaughlin and later by Brown in working with such weak signal levels pointed to the need to somehow raise these levels to workable values. The complex nature and uncertainties involved in the process by which SCR waves in TM modes negotiate the 20 degree bend in the slab and in leaving the tapered end transition to TE modes in the X-band waveguide was regarded as too difficult to analyze directly within the scope of this work. Instead it was decided to make a trial and error attempt to improve this transition in hopes of obtaining stronger signal levels. Several different designs were proposed for slabs which seemed, at least intuitively, to provide good beam-slab interaction while joining the waveguide without requiring the latter to be too closely located to the beam path. More STYCAST was ordered from which to fabricate these designs. Also, a Waveguide Mixer Adapter for the Tektronix S/A was located. This device is used with the S/A

to allow efficient input of signals in the 12.4 to 40 GHZ range.

The signals detected during the earlier experiments were input to the S/A using a Coaxial Adapter. A 2 foot coaxial cable connected a stub antenna inside the end of the waveguide to the S/A. The coaxial adapter is recommended by the manufacturer for inputting signals in the 1.5 to 12.4 GHZ range. While awaiting the arrival of the new STYCAST, it was decided to repeat the measurements made by Brown using the 20 degree bend slab but utilizing the waveguide mixer adapter to make the detection of higher frequencies possible. With the beam on, the procedure used was to search the 1.5 to 12.4 GHZ range with the coaxial adapter in place (although only signals above the 6.56 GHZ waveguide cutoff were expected), then to replace the coaxial adapter by the waveguide mixer adapter and search the 12.4 to 40 GHZ range. While first using this method a faulty coaxial connector was discovered in the line attached to the coaxial adapter. Since this equipment was used in the previous experiments and there was no reason to suspect that the fault did not exist unnoticed earlier, it is likely that this connector attenuated the signals seen by McLaughlin and Brown. In any event, it was found that with the S/A tuned to a strong signal the defective connector produced the same reduction in signal strength as a 20 dB attenuator internal

to the S/A which could be switched into the input path. Because the earlier signals were near the minimum sensitivity of the S/A an attenuation of this magnitude would have been serious enough to prevent detection of all but the strongest signals. While it may be pointless to speculate about what the effects of this defective part may have been on the earlier experiments it appears to have been significant when considering that the veritable plethora of signals detected here were obtained using essentially the same setup.

Figures 8 and 9 show two other geometries which were tested. One used STYCAST and another used polyethylene. The spectrum of observed frequencies did not seem to vary consistently with geometry but this is not surprising since the designs had essentially the same thickness and this is the only dimension which according to (3) is expected to affect the resonant behavior of the slab. Also, the strong signals detected (some required use of the internal attenuators to be on scale) following discovery of the faulty connector eliminated the immediate need to test other geometries for improved output transition characteristics.

C. RESULTS

Table I shows the frequencies detected using the 20 degree bend STYCAST slab and a 100 Mev beam. The material

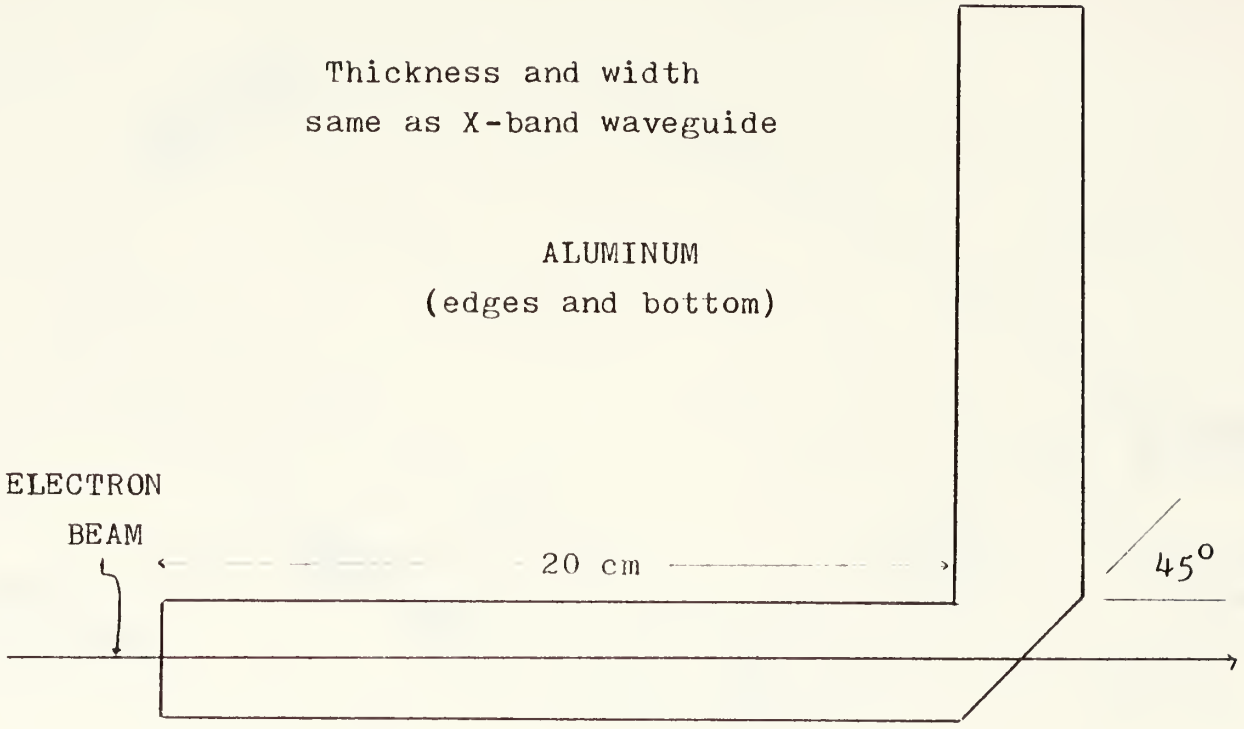

90 DEGREE BEND X-BAND STYCAST SLAB (TOP VIEW)

FIGURE 8

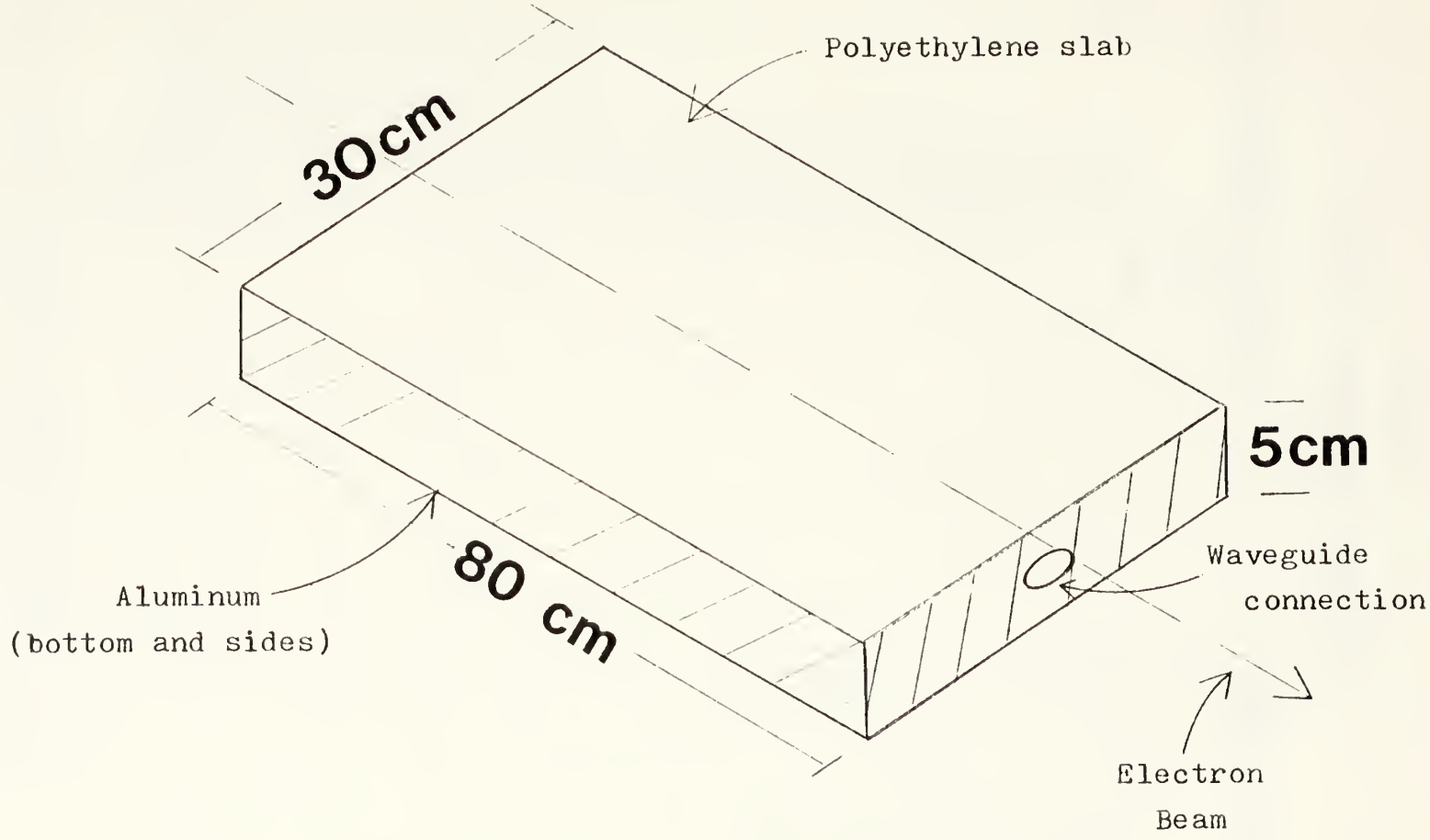

POLYETHYLENE SLAB

FIGURE 9

TABLE I

EMITTED FREQUENCY SPECTRUM

FREQUENCIES EMITTED BY SLAB			LINAC HARMONICS	
CA*		WMA†	#	
8.49 GHZ		18.0 GHZ	1	2.85 GHZ
8.55 (3)		19.05	2	5.70
8.59		19.27	3	8.55
10.25		19.61	4	11.4
11.50 (4)		19.83	5	14.25
		20.45	6	17.1
		20.58	7	19.95
		21.42	8	22.8
		21.47	9	25.65
		21.53	10	28.5
		21.78	11	31.35
		21.99	12	34.2
		22.20	13	37.05
		22.49	14	39.9
		22.86 (7)		
		23.12		
		23.45		
		23.85		
	12.20/24.55			
	12.42/25.1			
	12.64/25.49 (9)			
	12.88/25.97			
(5)	14.28/28.78 (10)			
	14.61/29.45			
	15.05/30.50			
	16.31/32.81			
	16.45/33.10			
	16.61/33.45			
	16.66/33.55			
(6)	17.18/35.90			
	17.84/35.90			
	17.98/36.10			
	18.00/36.2			
		38.25		
		38.81		

* Spectrum Analyzer Coaxial Adapter Input

† Spectrum Analyzer Waveguide Mixer Adapter Input

downstream of the bend was actually polyethylene since insufficient STYCAST had initially been available. For poly, n = 1.461, however it is not known what if any fraction of this section should be considered as taking part in the resonant process occurring in the straight 20cm section since the poly did not lie beneath the beam. The left column of Table I shows signals detected using the coaxial adapter. The middle column shows those found in the range of the waveguide mixer adapter. The right column lists the harmonics of the 2.85 GHZ LINAC RF frequency up to number 14 which is the highest order harmonic below the maximum detectable S/A frequency of 40 GHZ. More will be said later about these harmonics; however, the data of Table I show that the slab emitted at or very near virtually every LINAC harmonic with the exception of the first and second which are not propagated by the X-band waveguide. The number of the harmonic suspected to produce signals in the first two columns of Table I is indicated in parentheses.

The waveguide mixer adapter column of Table I contains several double entries. The operational features of the S/A basically prevented determining which of the two frequencies the S/A was tuned to, meaning that one or both of the frequencies listed may have been detected. This rather

confusing and ambiguous aspect of S/A operation and its implications are discussed in Chapter IV.

Two other versions of the 20 degree bend slab were tested using STYCAST. One used a shortened 10cm resonator and the other a longer 30cm resonator section. These both generated spectra which were identical to that of Table I within the accuracy of the equipment. A design employing a 90 degree bend shown in Figure 8 was tested. This design had the same thickness and width as the interior of the X-band waveguide and produced the data of Table II.

The poly slab of Figure 9 was the largest resonator used and was enclosed on every side except the top with aluminum. The waveguide pick off for this configuration was in line with the beam however and the antenna and air Cerenkov reception problems encountered before rendered this design unuseable as an SCR source.

As a check, an air Cerenkov spectrum was recorded using the open-ended waveguide in the same position relative to the beam path as when connected to the 20 degree bend slab. This produced the data of Table III which includes frequencies up to 40 GHZ. This had not been done in earlier experiments since the waveguide mixer adapter had been unavailable.

TABLE II

90 DEGREE BEND X-BAND STYCAST SLAB

COAXIAL ADAPTER	WAVEGUIDE MIXER ADAPTER
8.2 GHZ	24.3 GHZ
8.54	24.51
11.45	24.52
12.57	25.0
	13.25/26.75
	13.68/27.55
	13.80/27.8
	13.88/27.95
	14.18/28.52
	14.22/28.65
	14.28/28.76
	14.50/29.18
	14.90/30.0
	16.88/33.9
	17.18/34.55
	17.50/35.2
	17.90/36.05
	37.6
	38.6
	39.7

TABLE III

AIR CERENKOV SPECTRUM

COAXIAL ADAPTER	WAVEGUIDE MIXER ADAPTER
8.6 GHZ	12.2 /24.63 GHZ
11.5	12.63/25.47
	12.9 /25.9
	14.22/28.6
	14.35/28.4
	14.63/29.5
	15.14/30.48
	16.31/32.91
	17.2 /34.6
	17.8 /35.9
	18.0 /36.2
	38.8

IV. DISCUSSION

A. SPECTRUM ANALYZER CHARACTERISTICS

Because the S/A was used to obtain virtually all the data and in some cases produced ambiguous readings, a brief explanation of its operation is called for. The analyzer is tuneable from 10 MHZ to 40 GHZ. The input signal is heterodyned with a local oscillator and compared to an intermediate frequency oscillator. The mixers and other circuit components used produce images and harmonics of the actual input signal but these undesired signals can be identified through careful observation of their behavior in response to a change in local oscillator frequency as the tuner is adjusted. However, there is yet another shortcoming which is not so easily overcome. Figure 10 shows the S/A control panel and Figure 11 is a close-up of the tuner section. The dial scales are calibrated to the harmonics of the local oscillator fundamental [Ref. 10: p. 2-19]. With the scale select switch in position C, bands 4 through 8 which cover the frequency range 1.5 to 40 GHZ are monitored. As shown in Figure 11, the reticle is aligned with all the bands meaning that the operator must have some prior knowledge of the range in which detected signals are to be expected or some means of determining which of the indicated frequencies

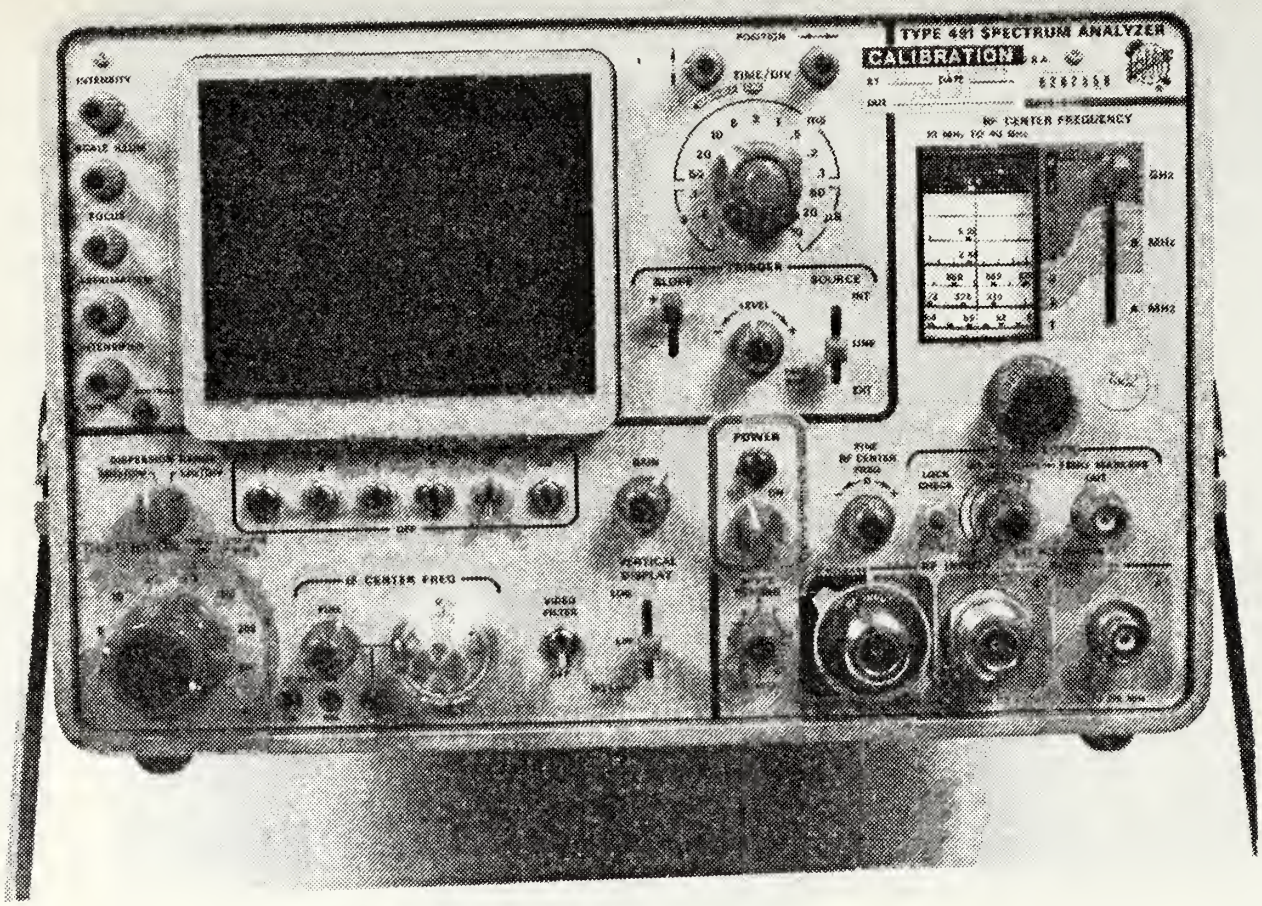

SPECTRUM ANALYZER CONTROLS

FIGURE 10

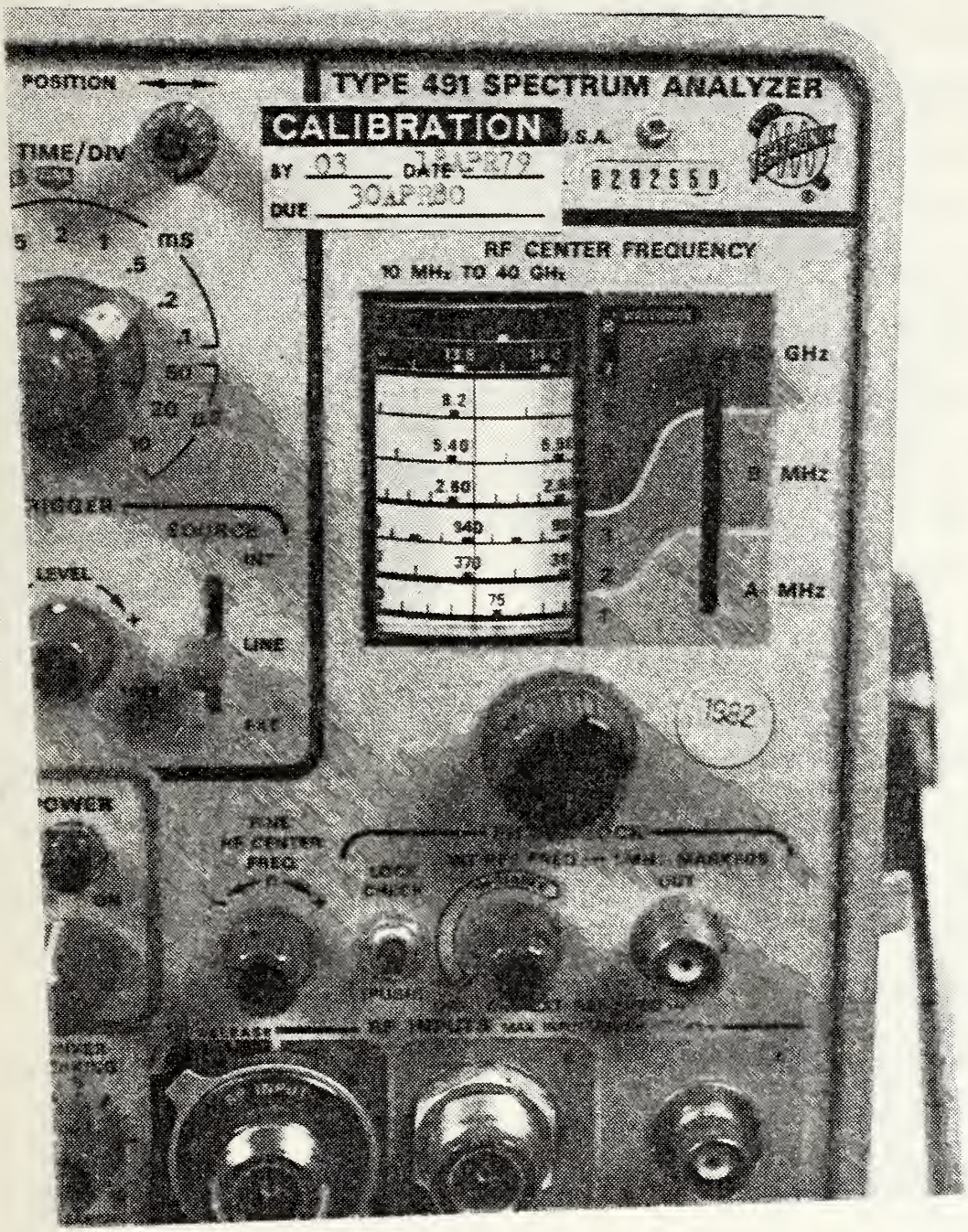

SPECTRUM ANALYZER TUNER SECTION

FIGURE 11

represents the correct value. The analyzer displays amplitude versus frequency. The extent of frequency displayed along the horizontal display (referred to as the frequency window) is adjustable by means of the dispersion control switch which offers several settings from 1 KHZ/div to 10 MHZ/div. With a display scale of ten divisions, this gives a maximum full scale frequency window of 100 MHZ or 0.1 GHZ. The normal procedure recommended by the manufacturer for resolving the ambiguity is to check for signal frequency shifts across the frequency window which are coincident with RF center frequency change as the tuner is adjusted. For example, with a dispersion setting of 5 MHZ/div (50 MHZ window) suppose that a signal is detected which is believed to be at 65 MHZ as indicated in band 1. Now, if the signal moves horizontally across the full window of 50 MHZ as the RF center frequency tuner is changed from 65 to 90 MHZ (a change of 25 MHZ), then the band 1 indication is erroneous and the next higher band should be read to determine the signal frequency. Unfortunately, when this procedure is attempted in bands 7 and 8 (12.4 to 40 GHZ) where the majority of signals from the slab are found, a new difficulty arises. Since the maximum full scale frequency window width is 0.1 GHZ, the effects of tuning most signals across the horizontal frequency scale in these bands produces such a small change in the indicated frequency that

reliable readings cannot be made. Most of the signals detected were broad enough to cover a large portion of the display at this dispersion setting which further added to the problem. For the above reasons it was not possible to resolve some ambiguities and some entries in the tables of Chapter III contain two values. Perhaps the most effective solution to this problem would be to use short sections of waveguide having cutoff frequencies matched to the upper frequency limits of band 6 and 7 so that once the S/A was tuned to a signal it could be conclusively associated with one band of indication by inserting the waveguide filter sections successively. The design and fabrication of such filters was not attempted, however, an existing section of K-band waveguide having a 9.4 GHZ cutoff frequency was used in line with signals input using the waveguide mixer adapter and demonstrated the practicality of this approach by blocking low band 6 signals when searching in only bands 7 and 8. Certainly the use of filters of this type would be a recommendation to future users of the S/A for this application.

B. THEORETICAL POWER SPECTRUM OF CERENKOV RADIATION IN AIR

The theory for the power generated in the dielectric waveguide by the LINAC beam has not been developed. It may be useful to compare the experimental results for a

dielectric waveguide with a known theory for Cerenkov radiation produced by periodic bunches of electrons in air.

F. R. Buskirk and J. R. Neighbours showed that the Cerenkov radiation intensity for a bunched 100 Mev beam in air should be coherent microwaves at harmonics of the bunch frequency with power rising with frequency until the wavelength emitted approaches the bunch length (.525cm or 57 GHZ for the NPS LINAC) (see Appendix A). Above this frequency then, the bunches radiate incoherently as electrons in a continuous beam would do. The power spectra of Figures 3 through 6 depict only the coherent radiation according to equation (10). Equation (10) also shows that the slope of the function P_ω involves q, the bunch charge, and other quantities which are known. The straight line behavior of the P_ω curves exhibited near $\omega = 0$ suggests that the slope could be most accurately evaluated in this region and (10) could be used to find q. Buskirk and Neighbours also showed that the radiation from the bunched beam in air should have a strong harmonic content up to the 20th order (see Appendix A) which is beyond the measuring capability of the available equipment. The data of Chapter III support this result and it is reasonable to expect that SCR produced in the beam-slab interaction behaves similarly (regarding harmonic content) to the normal Cerenkov produced in air. The harmonic content of the air Cerenkov spectrum

was successfully demonstrated by A. Saglam in support of Buskirk and Neighbour's work [Ref. 8]. Comparison of Tables I and III shows clearly that the signal emitted by the slab contained not only trapped air Cerenkov and its harmonics, but also other harmonics present only in the slab and believed to be SCR produced by evanescent coupling of the beam to the slab.

The radiated power and form factor calculations of Chapter II, Part B demonstrate the manner in which various changes in bunch charge distribution are expected to affect the radiation emitted in air. Figure 12 depicts electrons being carried along by RF waves in the LINAC. If the electrons are evenly distributed in phase with respect to the wave, then the LINAC magnet-slit structure described in Appendix A will produce square bunches, i.e., ones for which all regions along the 17.5 psec or .525cm long pulse contain the same number of electrons. Normally the LINAC prebuncher and space charge effects will give an uneven distribution of electrons with respect to the wave so that as the beam is bent and swept past the slit, a bunch will emerge having a charge distribution which varies spatially. Figure 13 shows possible square, Gaussian and cosine charge distributions which could result. The radiated power calculations of Appendix B suggest that of the types considered, the bunches having the cosine charge distribution radiated most

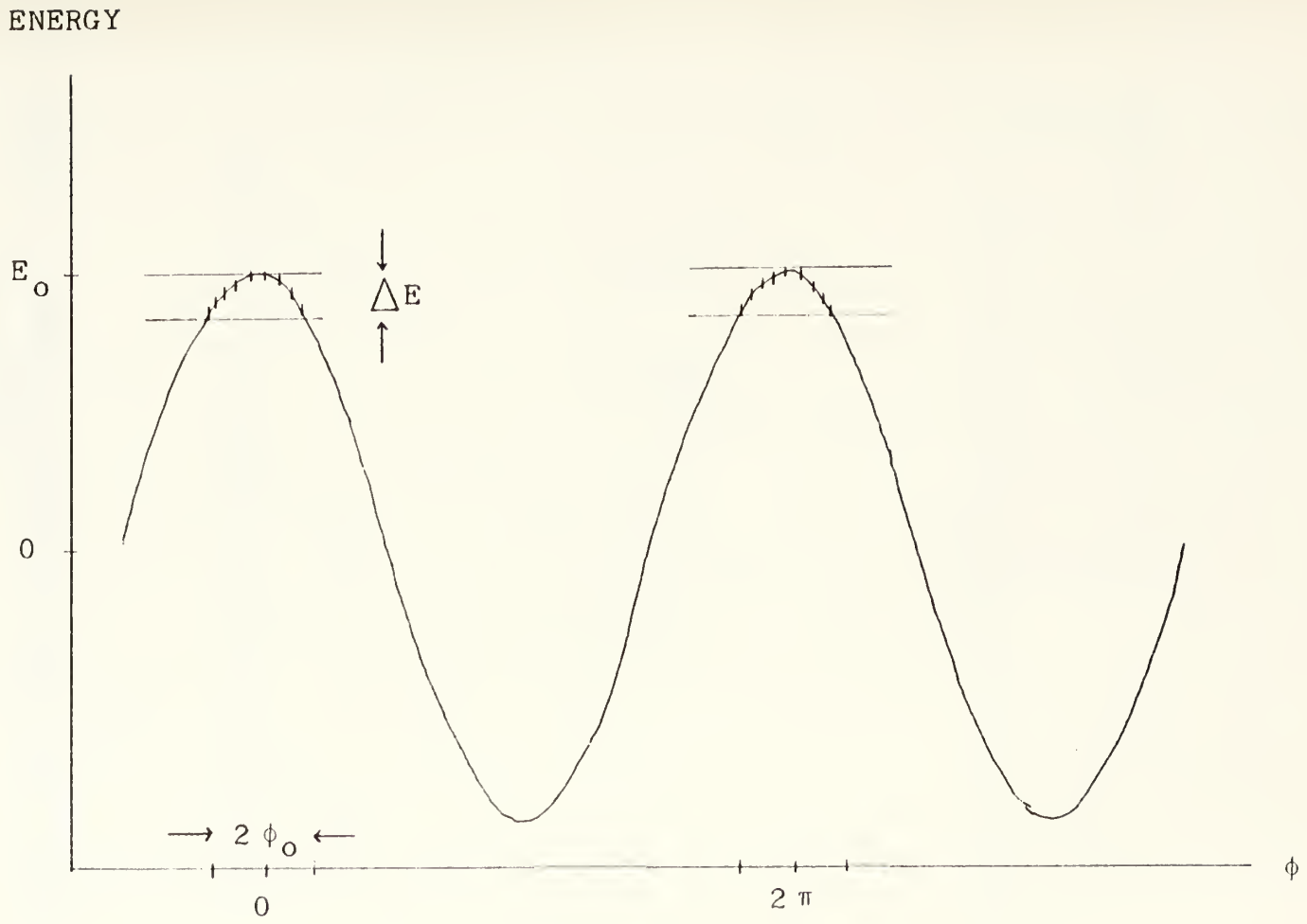

FIGURE 12. STRUCTURE OF CHARGE PULSE FROM A TRAVELING WAVE ACCELERATOR. ϕ is the phase angle of an electron relative to the peak of the wave. Electrons in the range $\pm\phi_o$ are passed by a magnetic deflection system.

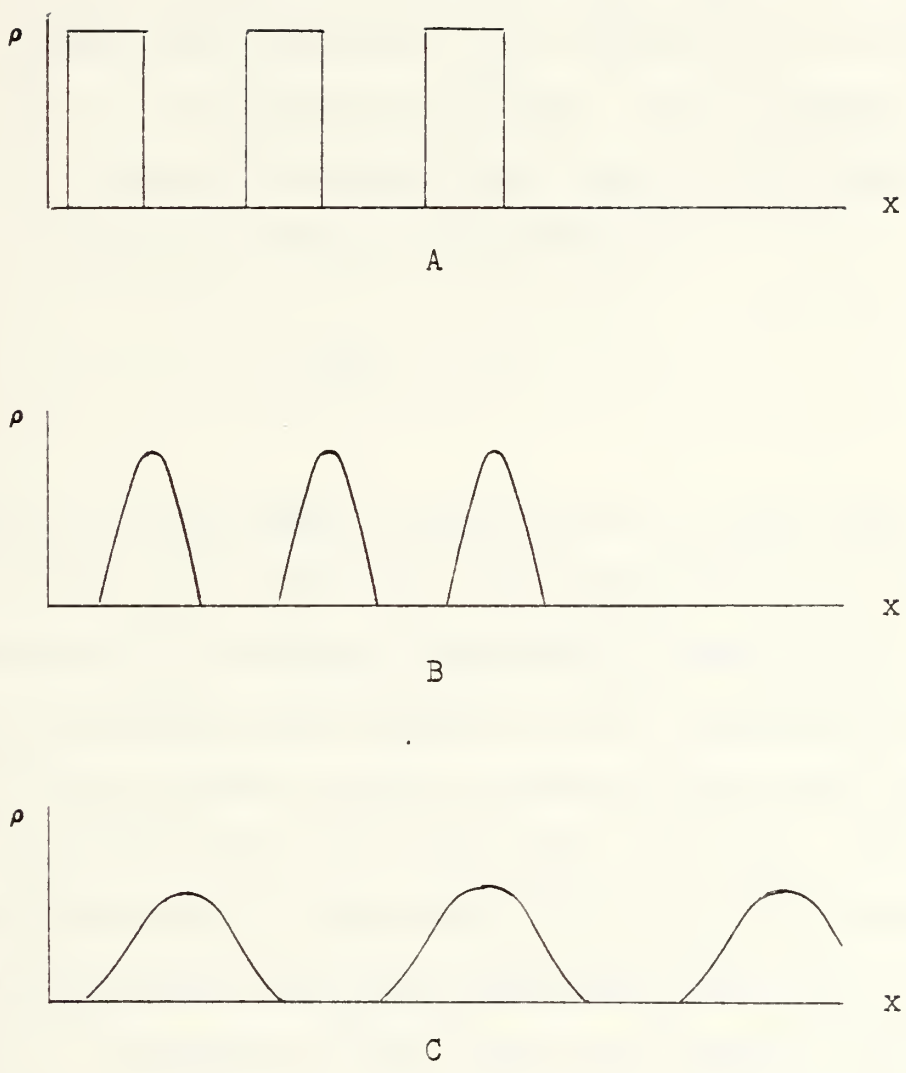

FIGURE 13. POSSIBLE ELECTRON BUNCH STRUCTURES.

A. Uniform

B. Cosine

C. Gaussian

efficiently and produced the highest peak power level. This is because this type distribution concentrates more charge near the center of the bunch than the other types. In Appendix B the frequency at which the peak power occurs is seen to depend upon the ratio r_o/v where r_o is the bunch radius and v is the electron velocity. As an example, the peak in the coherent radiated power from uniform spherical bunches is shown in Figure 3 to occur for

$$\frac{\omega r_o}{v} = 1.6$$

Taking v as the speed of light and r_o as 1cm gives $\omega = 48 \times 10^9$ or f = 7.64 GHZ. Since the value of v will vary little for high energy electrons the value of r_o actually determines the frequency of peak radiated power. Because of the inverse relation between these quantities, doubling r_o would halve the peak power frequency. This dependence also would allow the value of r_o to be determined experimentally from a radiated power spectrum such as that of Figure 3, although as shown above the typical frequencies required to measure such a spectrum may extend beyond the capabilities of the equipment used here. If such a spectrum were obtained experimentally it is reasonable to ask whether the functional form of $\rho(r)$ could be determined from this information. In practice this could be a very difficult

task even for the simple forms of $\rho(r)$ used as examples here. An actual accelerator is likely to produce bunches having much more complex charge distributions and it is doubtful that a solution could be achieved in most cases. Still, the radiated power curve should allow the determination of bunch charge and size and give a qualitative insight into the type charge distribution by comparison to previously analyzed examples since the physical process producing the bunches more or less requires that they have some shape similar to an elongated spheroid.

C. CONCLUSION

The results confirmed the production of SCR; however, the failure of the theory to give the actual frequencies observed indicates that the beam-to-slab evanescent coupling process is not understood correctly. To its credit, the theory did predict that for a given beam and slab, SCR should depend on only slab thickness. The data taken using different materials and geometries confirmed this point in so far as changes in other slab parameters did not affect the output radiation. The relatively crude apparatus produced sufficient signal strength to allow monitoring approximately 75 feet away from the slab and equation (1) suggests that stronger signals can be obtained by increasing the beam-slab interaction distance. In Part B above it is shown that much of the radiated power was probably at

frequencies too high to be detected. Also, the spectrum of frequencies observed was in qualitative agreement with the type harmonic behavior predicted by Buskirk and Neighbours for air Cerenkov from a bunched beam.

A practical use for a relativistic bunched beam monitor which does not disturb the beam has been identified for free electron lasers. A cylindrical resonator intended to produce high power microwave radiation has demonstrated successful operation [Ref. 3]. In a beam monitor, the goal would be to remove as little power from the beam as needed for diagnostic purposes. The theory suggests that the cylindrical resonator could be scaled down to operate at lower power levels. Reference 3 also gives evidence that the cylindrical geometry seems to couple to the beam more effectively than the slab. This at least agrees with intuition since the beam itself has cylindrical symmetry about its axis.

It therefore seems that the most promising direction to be taken for further research along these lines would involve the use of a scaled down version of a cylindrical resonator design similar to that described by Felch [Ref 3: p. 145-149]. This type resonator has already been coupled to an X-band waveguide with good results by using a brass stub which protruded from the resonator into the waveguide to launch TE modes. Although this design used a quartz

resonator, a cylinder made from STYCAST should work well. The relatively inexpensive fabrication of two short waveguide filters described earlier would greatly enhance the usefulness of the not so inexpensive spectrum analyzer already available. It should also prove worthwhile to make an effort to determine the upper limit in frequency of detectable radiation from the slab since this apparently extended beyond the useful range of the spectrum analyzer. If these steps are taken, the cylindrical resonator and spectrum analyzer should be useable as a prototype beam monitor. The next step would be to take the data to construct as much of the radiated power curve as possible and compare to the behavior predicted by equation (10) for normal air Cerenkov with the ultimate goal of determining bunch charge, size, and charge distribution.

APPENDIX A

NAVAL POSTGRADUATE SCHOOL LINEAR ACCELERATOR

The linear accelerator (LINAC) used for this experiment produces a bunched electron beam rather than a continuous one. Three klystron tubes are used to individually provide power to each of three ten foot long accelerating sections of the Stanford type. An electron gun at the beginning of the accelerator injects electrons at roughly $\beta = .5$. The design of the accelerator sections causes the RF energy to propagate in a TM mode. This produces a component of electric field in the longitudinal direction which is thus available for accelerating electrons. For the present, we are interested not so much in the accelerator itself as in the beam it produces.

The injected electrons are quickly accelerated to near the velocity of light in their first few centimeters of travel. From this point on they essentially gain mass and energy as the velocity increases very little. The increase in mass "stiffens" the beam and fortuitously simplifies the job of keeping the beam straight within the accelerator where mechanical tolerances are small.

The acceleration experienced by an individual electron is dependent on its location with respect to the RF wave.

Figure 12 depicts this situation. Although the LINAC design incorporates a prebuncher [Ref. 11: p. 37-38] which seeks to minimize the waste of injected electrons, an unavoidable consequence of this method is that a spectrum of electron energies is produced. In order to narrow this energy spectrum the highest energy electrons are separated from the others by first bending the beam with a magnet then using a tungsten slit to block electrons not having the desired energy. The bending process distributes the electrons according to energy in the same way that a glass prism spreads white light into the various energy components we usually think of as colors. As might be expected, the high energy electrons which impinge on the tungsten slit are the major source of gamma and x-ray radiation produced by the LINAC.

It is easy to understand how picking off only the electrons riding the crests of the waves in Figure 12 leads to a bunched beam. If we let ϕ be the phase of an electron relative to the peak of the wave, then the phase of an arbitrary electron can be expressed as

$$E = E_o \cos \phi \qquad (A1)$$

where E_o is the maximum electron energy. We assume that the magnet is adjusted so that only electrons having energies between E_o and $E_o - \Delta E$ are accepted by the slit.

We also assume that in order to have this energy, an electron must be riding within $\pm\phi_o$ of the crest. Then, the energy of the least energetic electrons which emerge from the slit is

$$E_o - \Delta E = E_o \cos \phi_o \tag{A2}$$

$$1 - \frac{\Delta E}{E_o} = \cos \phi_o \tag{A3}$$

$$= 1 - \frac{\phi_o^2}{2} \quad \text{(for } \phi_o \text{ small)} \tag{A4}$$

$$\frac{\phi_o^2}{2} = \frac{\Delta E}{E_o} \tag{A5}$$

For the NPS LINAC, one percent energy resolution is used. Therefore, (A5) becomes

$$\frac{\Delta E}{E_o} = .01 = \frac{\phi_o^2}{2}$$

$$\phi_o^2 = .02$$

$$\phi_o = .14 \text{ radian}$$

$$\frac{2\phi_o}{2\pi} = .05 \tag{A6}$$

Equation (A6) states that electrons which have the proper energy exist for only 5% of the RF cycle giving a bunch duration of

$$\frac{.05}{2.856 \text{ GHZ}} = 17.5 \text{ psec}$$

The RF wave period of 350.14 psec is 20 times longer than the bunch duration time which means that the fourier expansion for the beam current should have a strong harmonic content up to the 20th order. In fact, the beam is further structured because of the fact that the klystrons are unable to continuously keep the accelerator filled with the amount of RF energy needed and must therefore be pulsed. One microsecond pulses are repeated 60 times per second giving each microsecond beam pulse a total of 2856 bunches.

Incidentally, the 2.856 GHZ RF gives the bunches a separation of 10.5cm while the bunch duration of 17.5 psec gives them a length of .525cm. Here again the 20/1 ratio is preserved and is a direct result of the design energy resolution criterion.

APPENDIX B

RADIATED POWER CALCULATIONS

In this appendix, form factors and coherent radiated power are calculated for bunch types other than the uniform spherical example of the main text. The specific examples used are bunches having radial charge distributions described by cosine, Gaussian and spherical shell functions.

A. COSINE BUNCH

Let the bunch charge distribution be dependent only on r so that in spherical coordinates it can be described by

$$\rho(r) = \rho_o \cos br$$

Then the bunch charge q is found as follows:

$$q = \iiint \rho_o \cos br \, d^3r$$

$$= 4\pi\rho_o \int_0^{\frac{\pi}{2b}} r^2 \cos br \, dr$$

$$= 4\pi\rho_o \left[\frac{2r}{b^2} \cos br + \left(\frac{r^2}{b} - \frac{2}{b^3} \right) \sin br \right]_0^{\frac{\pi}{2b}}$$

$$= 4\pi\rho_o \left(\frac{\pi^2}{4b^3} - \frac{2}{b^3} \right)$$

Using the definition of F(k) from the main text,

$$F(k) = \frac{1}{q} \iiint d^3r\ \rho(r) e^{ik\cdot r}$$

$$= \frac{1}{q} \iiint r^2 dr \sin\theta d\theta d\phi \rho(r) e^{ikr\cos\theta} \qquad \text{(B1)}$$

Continuing from equation (B1), let

$$u = \cos\theta$$

$$du = \sin\theta d\theta$$

$$F(k) = \frac{2\pi}{q} \iint e^{ikru}\ r^2\ \rho(r) du dr$$

$$= \frac{2\pi}{q} \int \frac{2}{kr} \sin kr\ r^2\ \rho(r) dr$$

Substituting for $\rho(r)$ and adding the limits on r gives

$$F(k) = \frac{4\pi\rho_o}{qk} \int_0^{\frac{\pi}{2b}} r \sin kr \cos br\ dr$$

$$= \frac{4\pi\rho_o}{qk} \int_0^{\frac{\pi}{2b}} \frac{r}{2} [\sin(b+k)r - \sin(b-k)r]\ dr$$

$$= \frac{4\pi\rho_o}{qk} \left[\frac{\frac{\pi k}{2b} \sin\frac{\pi k}{2b}}{(b^2 - k^2)} - \frac{2bk \cos\frac{\pi k}{2b}}{(b^2 - k^2)^2} \right]$$

Substituting for q gives

$$F(k) = \frac{1}{\left(\frac{\pi}{2}\right)^2 - 2}\left\{\frac{\frac{\pi}{2}\sin\frac{\pi k}{2b}}{\frac{k}{b}\left[1-\left(\frac{k}{b}\right)^2\right]} - \frac{2\cos\frac{\pi k}{2b}}{\left[1-\left(\frac{k}{b}\right)^2\right]^2}\right\}$$

Now we use $k = \omega/v$ and equation (10) from before to find P_ω.

$$P_\omega = \frac{\mu}{4\pi}\omega_o v \sin^2\theta_c q^2 N_\omega \left\{\frac{1}{\left(\frac{\pi}{2}\right)^2 - 2}\left[\frac{\frac{\pi}{2}\sin\frac{\pi\omega}{2vb}}{\frac{\omega}{vb}\left[1-\left(\frac{\omega}{vb}\right)^2\right]} - \frac{2\cos\frac{\pi\omega}{2vb}}{\left[1-\left(\frac{\omega}{vb}\right)^2\right]^2}\right]\right\}^2 \quad (B2)$$

B. GAUSSIAN BUNCH

$$\rho(r) = \rho_o e^{-\left(\frac{r}{a}\right)^2}$$

$$F(k) = \frac{\iiint \rho_o e^{ik\cdot r} e^{-\left(\frac{r}{a}\right)^2} d^3r}{\iiint \rho_o e^{-\left(\frac{r}{a}\right)^2} d^3r}$$

$$= \frac{a^3 \rho_o \pi^{\frac{3}{2}} e^{-\left(\frac{ka}{2}\right)^2}}{a^3 \rho_o \pi^{\frac{3}{2}}}$$

$$= e^{-\left(\frac{ka}{2}\right)^2}$$

$$P_\omega = \frac{\mu}{4\pi}\,\omega_o\, v\, \sin^2\theta_c q^2 N\omega\; e^{-\frac{1}{2}\left(\frac{\omega a}{v}\right)^2} \qquad \text{(B3)}$$

C. SPHERICAL SHELL

$$\rho(r) = f\,\delta(r - r_o)$$

$$q = \iiint \rho(r)\, d^3r$$

$$= 4\pi \int_0^\infty r^2 \quad f\,\delta(r - r_o)\, dr$$

$$= 4\pi\, f\, r_o^2$$

$$F(k) = \frac{1}{q}\,\frac{4\pi}{k} \int_0^\infty r \quad f\,\delta(r - r_o)\, \sin kr\, dr$$

$$= \frac{4\pi}{qk}\, r_o\, f\, \sin kr_o$$

Substituting for q gives

$$F(k) = \frac{\sin kr_o}{kr_o}$$

$$P_\omega = \frac{\mu}{4\pi}\,\omega_o\, v\, \sin^2\theta_c q^2 N\omega \left[\frac{\sin\frac{\omega r_o}{v}}{\frac{\omega r_o}{v}}\right]^2 \qquad \text{(B4)}$$

D. NORMALIZATION

Since we wish to be able to compare the results for the four type bunch charge distributions we choose the uniform spherical bunch and require the other bunches to have the same total charge and size. In the case of the cosine distribution, this requirement specifies the parameter b in terms of r_o of the uniform bunch:

$$b = \frac{\pi}{2r_o}$$

For the Gaussian distribution we choose the parameter a such that

$$\rho(r = a) = \frac{1}{10}\,\rho(r = 0)$$

$$\rho_{Go}\left\{e^{-\frac{r^2}{a^2}}\right\} = \frac{1}{10}\,\rho_{Go}$$

$$a = \frac{r_o}{\sqrt{\ln 10}}$$

The spherical shell distribution is considered to concentrate its charge in a shell having the same radius, r_o, as the uniform bunch.

When these substitutions are made, equations (10) from the text and (B2) through (B4) are all expressed in terms of r_o as follows: To simplify these expressions, we have let

$$A = \frac{\mu}{4\pi} \omega_o v \sin^2\theta_c q^2 N$$

and

$$\frac{\dot{r}_o}{v} = 1$$

$$P_{\omega_{uniform}} = A\omega \left[3\left(\frac{v}{\omega r_o}\right)\left(\sin \frac{\omega r_o}{v} - \frac{\omega r_o}{v} \cos \frac{\omega r_o}{v}\right) \right]^2$$

$$= A\omega \left[\frac{3}{\omega^3} \left(\sin\omega - \omega\cos\omega\right)\right]^2$$

$$P_{\omega_{cosine}} = A\omega \left[\frac{1}{\frac{\pi^2}{2} - 2} \left\{ \frac{(\frac{\pi}{2})^2 \sin\omega}{\left(1 - (\frac{2}{\pi})^2 \omega^2\right)} - \frac{2\cos\omega}{\left(1 - (\frac{2}{\pi})^2 \omega^2\right)^2} \right\} \right]^2$$

$$P_{\omega_{Gaussian}} = A\omega e^{-\frac{1}{2}\frac{1}{\ln 10}\omega^2}$$

$$P_{\omega_{shell}} = A\omega \left(\frac{\sin\omega}{\omega}\right)^2$$

These functions are plotted in Figures 3 through 6 of the text in terms of $\frac{\omega r_o}{v}$. For example, if $\frac{\omega r_o}{v} = 1$ and we take r_o to be 1 cm and v = c, then

$$\omega = \frac{v}{r_o} = \frac{3 \times 10^{10} \text{ cm/sec}}{1 \text{ cm}} = 3 \times 10^{10} \text{ radian/sec}$$

$$f = \frac{\omega}{2\pi} = 4.77 \text{ GHZ}$$

LIST OF REFERENCES

1. Walsh, J. E., Stimulated Cerenkov Radiation, Department of Physics and Astronomy, Dartmouth College, Hanover, New Hampshire.

2. Jelley, J. V., Cerenkov Radiation, Pergamon Press, 1958.

3. Felch, K. L., Cerenkov Radiation in Dielectric Loaded Waveguides, Ph.D. Thesis, Dartmouth College, Hanover, New Hampshire, 1980.

4. Walsh, J. E.; Marshal, T. C.; Schlesinger, S. P.; "Generation of Coherent Cerenkov Radiation with an Intense Relativistic Electron Beam," Physics of Fluids, Vol. 20, No. 4, p. 709-710, April 1977.

5. McLaughlin, D. E., Cerenkov Radiation Produced by 100 Mev Electrons, M.S. Thesis, Naval Postgraduate School, Monterey, California, June 1981.

6. Brown, L. J., Stimulated Cerenkov Radiation Produceed by 100 Mev Electrons, M.S. Thesis, Naval Postgraduate School, Monterey, California, December 1981.

7. Naval Postgraduate School Technical Report NPS-61-83-003. Cerenkov Radiation from Bunched Electron Beams, by F. R. Buskirk and J. R. Neighbours, revision 1, April 1983.

8. Saglam, A., Cerenkov Radiation, M.S. Thesis, Naval Postgraduate School, Monterey, California, December 1982.

9. Skilling, H. H., Fundamentals of Electric Waves, Krieger Publishing Co., 1974.

10. Tektronix Inc. Technical Manual, Type 491/491R Spectrum Analyzer, Bremerton, Oregon, August 1974.

11. Barnett, M. T., Jr. and Cunneen, W. J., Design and Performance of Electron Linear Accelerator at the U.S. Naval Postgraduate School, M.S. Thesis, Naval Postgraduate School, Monterey, California, May 1966.

12. Fowles, G. R., Introduction to Modern Optics, Holt, Rinehart and Winston, 1975.

INITIAL DISTRIBUTION LIST

		No. copies
1.	Defense Technical Information Center Cameron Station Alexandria, Virginia 22314	2
2.	Library, Code 0142 Naval Postgraduate School Monterey, California 93940	2
3.	Physics Library, Code 61 Department of Physics Naval Postgraduate School Monterey, California 93940	1
4.	Professor F. R. Buskirk, Code 61Bs Department of Physics Naval Postgraduate School Monterey, California 93940	4
5.	Professor J. R. Neighbours, Code 61Nb Department of Physics Naval Postgraduate School Monterey, California 93940	1
6.	LT. K. S. Pugh 1025 Audubon LN Lake Charles, Louisiana 70605	1

201690
Thesis
P94763 Pugh
c.1 Stimulated Cerenkov
radiation beam monitor.